A comparison of three explicit local meshless methods using radial basis functions

Guangming Yao [a,*], Bozidar Šarler [b], C.S. Chen [c]

[a] IMPOL Aluminium Industry, Slovenska Bistrica, Slovenia
[b] Laboratory for Multiphase Processes, University of Nova Gorica, Slovenia
[c] Department of Mathematics, University of Southern Mississippi, MS 39406, USA

ARTICLE INFO

ABSTRACT

In this paper, three kinds of explicit local meshless methods are compared: the local method of approximate particular solutions (LMAPS), the local direct radial basis function collocation method (LDRBFCM) which are both first presented in this paper, and the local indirect radial basis function collocation method (LIRBFCM). In all three methods, the time discretization is performed in explicit way, the multiquadric radial basis functions (RBFs) are used to interpolate either initial temperature field and its derivatives or the Laplacian of the initial temperature field. The five-noded sub-domains are used in localization. Numerical results of simple diffusion equation with Dirichlet jump boundary condition are compared on uniform and random node arrangement, the accuracy and stabilities of these three local meshless methods are asserted. One can observe that the improvement of the accuracy with denser nodes and with smaller time steps for all three methods. All methods provide a similar accuracy in uniform node arrangement case. For random node arrangement, the LMAPS and the LDRBFCM perform better than the LIDRBFCM.

1. Introduction

During the last two decades the meshless methods have been developed and effectively applied to solve many engineering and science problems [1–4]. There are plenty of meshless methods under development [5–7]. There is a class of meshless methods that focus on the use of radial basis functions [8], such as radial basis function collocation method (RBFCM) [9–13]. The radial basis functions (RBFs) have been first under intensive research in multivariate data [12] and function interpolation [14]. Kansa used them for scattered data approximation in [12] and pioneered the solution of PDEs [13], that is why the method is sometimes called the Kansa's method. The key point of the RBFCM or Kansa's method for solving the PDEs is the approximation of the fields on the boundary and in the domain by a set of global approximation functions. The main advantage of using the RBFCM for solution of PDEs is its simplicity, applicability to various PDEs, and effectiveness in dealing with high dimensional problems and complicated domains. The method has been recently applied to many scientific and engineering disciplines. It has been used in the heat transport context in 1998 by Zerroukat et al. [14], in the context of porous media flow by Šarler et al. [15] in 2000, in the classical De Vahl Davis natural convection problem [16] by a symmetric and modified collocation in 2005 by Šarler [17]. The main disadvantage of RBFCM represents the related full matrices that are very sensitive to the choice of the free parameter in RBFs and difficult to solve for problems with a large number of unknowns. This is because the use of the radial basis function interpolation increases the condition numbers of the related matrices with increasing number of nodes. This is especially true for bad choice of data centers and when infinitely smooth basic functions such as multiquadrics is used with extreme values of their associated shape parameter. There are several methods to circumvent this issue such as domain decomposition [18,19], the greedy algorithm [20,21], extended precision arithmetic [22], the improved truncated singular valued decomposition [23], etc.

One of the possibilities for mitigating computational cost for large-scale problems is to employ the domain decomposition by Mai-Duy and Tran-Cong [24], multi-grid approach and compactly supported RBFs by Chen et al. [25] in 2002, which all represent a substantial complication of the original simple method. To avoid fully populated matrices, various localized meshless methods have been recently developed, such as the local quadrature based RBF approach by Shu et al. [26] in 2003, local multiquadric approximation using large sparse matrix by Lee et al. [27], and other local meshless methods in [28,29]. Among them, the local RBF collocation method was developed by Šarler and Vertnik [28] in 2006, the main issue of the local version of the RBFCM is the

* Corresponding author.
E-mail address: guangmingyao@gmail.com (G. Yao).

collocation on a sub-set of, in general, overlapping sub-domains, which drastically reduces the collocation matrix size on the expense of solving many small matrices with the dimension of the number of nodes included in the domain of influence for each node instead of a large collocation matrix. Since the method does not experience significant accuracy drawback in comparison with the global version, it has been applied to many complex PDEs, industrial applications and large-scale problems.

In this paper, we focus on three explicit local collocation methods for solving heat diffusion equations. The first method is the localized method of approximate particular solutions (LMAPS) which is the localized version of the method of approximate particular solutions (MAPS). The global MAPS was developed for the variance coefficients elliptic problems in [30], the local formulation LMAPS will be presented in this paper and applied to time dependent problems. The second method is the direct local RBF collocation method (LDRBFCM). It was first introduced for diffusion problems in [28]. The results in the paper show the accuracy and efficiency. Many authors apply the LDRBFCM to more complex problems such as convection-diffusion problems with phase-change [31], continuous casting [32], solid–solid phase transformations [33], and Navier–Stokes equations [34], Darcy flow [35], turbulent flow [36], etc. The third method we are comparing is the indirect local RBF collocation method (LIRBFCM) which was introduced in 2002 by Mai-Duy et al. [37] in its global form. This method was used to approximate derivatives of original functions and a closed form of original function approximation can be obtained. The global DRBFCM and IRBFCM were compared for approximations of function and corresponding derivatives, the IRBFCM approach yields a superior accuracy with uniform nodes. In [38], the indirect method with thin plate splines RBF was studied. We localize the IRBFCM in this paper and apply it to diffusion equation. Overall, the LMAPS and the LIRBFCM are new techniques, which are explicit localized version of the MAPS in [30] and the IRBFCM in [37], respectively. The LDRBFCM was first introduced in [28] in 2006.

The organization of the paper is as follows. In Section 2, the governing equation is given. In Section 3, we give a brief introduction of explicit time stepping strategy, theoretical backgrounds of the LMAPS, the LDRBFCM, and the LIRBFCM are given. Extensive numerical comparisons in the sense of the accuracy and the stability of the three methods for the diffusion equation with Dirichlet jump boundary condition are given in Section 4 as a function of the number of nodes, the node distribution (uniform, non-uniform), and time step length. In Section 5, we draw conclusions regarding the assessment of the methods used.

2. Governing equations

Consider a dimensionless diffusion equation defined on domain Ω with boundary Γ

$$\frac{\partial T}{\partial t} = \nabla^2 T \tag{1}$$

with initial condition

$$T(\mathbf{p},t_0) = T_0, \quad \mathbf{p} \in \Omega \cup \Gamma \tag{2}$$

and Dirichlet boundary condition

$$T(\mathbf{p},t) = T_D, \quad t \geq t_0, \quad \mathbf{p} \in \Gamma. \tag{3}$$

Let Δt be the time step length. We seek the solution T of the governing Eq. (1) in Ω at time $t_0+\Delta t$ by assuming the initial condition (2) and boundary condition (3).

3. The three meshless methods using radial basis functions

In this section we structure the three local meshless methods: the LMAPS, the LDRBFCM and the LIRBFCM. Time stepping strategy is one of the most popular methods for obtaining numerical solutions of time dependent partial differential equations. For $t \in (t_0,t_0+\Delta t)$, the time discretization is made by the following approximation:

$$\frac{\partial T}{\partial t} \approx \frac{T-T_0}{\Delta t}, \quad \nabla^2 T \approx \nabla^2 T_0, \tag{4}$$

then T in (1) can be approximated as

$$T(\mathbf{p},t_0+\Delta t) \approx \hat{T}(\mathbf{p},t_0+\Delta t) = T_0 + \Delta t \nabla^2 T_0, \quad \mathbf{p} \in \Omega \cup \Gamma. \tag{5}$$

This is commonly used explicit time stepping strategy that approximates $T(\mathbf{p},t_0+\Delta t)$ by using entirely the temperatures at the initial time t_0 in Ω and the boundary condition at $t_0+\Delta t$ on Γ.

Throughout the paper, the following node notations are used. The points we choose in $\Omega \cup \Gamma$ are denoted by $\mathbf{p}_k$; $k=1,2,\ldots,N$, where N represents the total number of nodes. The region $\Omega \cup \Gamma$ is divided into N overlapping sub-domains, $_l\Omega$; $l=1,2,\ldots,N$. The schematic of the node distribution with typical sub-domains is shown in Fig. 1. Each of the sub-domains consists of $_lN$ points $_l\mathbf{p}$; that coincide with some of the global points $\mathbf{p}_k$; $k=1,2,\ldots,N$. There is a relation between the global and the local point with indexes on each of the sub-domains: $k=k(l,n)$. The $k(l,n)$ is a function of the local sub-domain index l and local index n. It follows that

$$\mathbf{P}_{k(l,n)} = {_l\mathbf{P}}; \quad l = 1,2,\ldots,N, \quad n = 1,2,\ldots,{_lN}. \tag{6}$$

For convenience, in this paper we will only focus on 2D case; i.e., for $\mathbf{p} \in \Omega$,

$$\mathbf{p} = (x,y). \tag{7}$$

3.1. Involved RBFs

In all the methods in this paper, the types of radial basis functions can be chosen as needed, but the corresponding differentiations and integrations are needed. They can be easily obtained by hand or by symbolic mathematical software. In this paper, we use the following multiquadrics (MQ) RBF:

$$\psi(r) = \sqrt{r^2+c^2} \tag{8}$$

in 2-D and the corresponding related functions are listed below.

For the LMAPS, the derivation of particular solution can be found in [40]

$$\phi(r) = \frac{1}{9}(4c^2+r^2)\sqrt{r^2+c^2} - \frac{1}{3}c^3 \ln\left(c+\sqrt{r^2+c^2}\right). \tag{9}$$
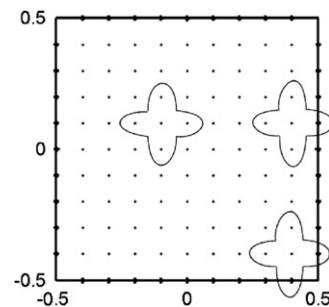
Fig. 1. The 11×11 uniform node arrangement and the schematics of the local domains of influence in interior, at the near boundary and at the corner using $_lN=5$.

For the LDRBFCM, by direct differentiation we have

$$\varphi(r) = \nabla^2 \psi(r) = \frac{r^2 + 2c^2}{(r^2 + c^2)^{1.5}}. \tag{10}$$

For the LIRBFCM [24],

$$\begin{aligned}
\varphi^{xx}(\mathbf{p}) &= \iint \psi(\|\mathbf{p} - \mathbf{p}_c\|) \, dx \, dx \\
&= \frac{1}{6}((x - x_c)^2 - 2(y - y_c)^2 - 2c^2)(r^2 + c^2)^{1/2} \\
&\quad + \frac{1}{2}(x - x_c)\left[(y - y_c)^2 + c^2\right] \ln\left[(r^2 + c^2)^{1/2} + (x - x_c)\right],
\end{aligned} \tag{11}$$

$$\begin{aligned}
\varphi^{yy}(\mathbf{p}) &= \iint \psi(\|\mathbf{p} - \mathbf{p}_c\|) \, dy \, dy \\
&= \frac{1}{6}((y - y_c)^2 - 2(x - x_c)^2 - 2c^2)(r^2 + c^2)^{1/2} \\
&\quad + \frac{1}{2}(y - y_c)\left[(x - x_c)^2 + c^2\right] \ln\left[(r^2 + c^2)^{1/2} + (y - y_c)\right].
\end{aligned} \tag{12}$$

3.2. LMAPS

In this approach, the formulation of the problem starts with the representation of the Laplacian of the original function (initial temperature field) with RBFs, the original function is then obtained by integration. Assume that

$$\nabla^2 T_0(\mathbf{p}) = \sum_{n=1}^{lN} \psi(\|\mathbf{p} - \mathbf{p}_{k(l,n)}\|)_l \alpha_n; \quad \mathbf{p} \in {}_l\Omega, \tag{13}$$

where ψ is a RBF and $\|\bullet\|$ is the Euclidean norm. For RBF $\psi(\|\mathbf{p} - \mathbf{p_c}\|)$ with the center $\mathbf{p_c} = (x_c, y_c)$, we denote

$$r = \|\mathbf{p} - \mathbf{p_c}\| = \sqrt{(x - x_c)^2 + (y - y_c)^2}. \tag{14}$$

Note that in 2-D case due to the symmetry of RBFs

$$\nabla^2(\psi(r)) = \frac{1}{r}\frac{d}{dr}\left(r\frac{d(\psi(r))}{dr}\right), \tag{15}$$

Then the inverse of Laplacian on RBF $\psi(r)$ is

$$\phi(r) = \int \frac{1}{r} \int r\psi(r) \, dr \, dr, \tag{16}$$

where $\nabla^2 \phi(r) = \psi(r)$. Note that the integration of (16) has to be treated with care. There are two arbitrary constants to be determined. In some cases such as MQ, one has to choose these two arbitrary constants in such a way to cancel the singularities [40]. The function $\phi(r)$ is called a particular solution for Laplacian operator ∇^2 with respect to the RBF $\psi(r)$. The Laplacian on temperature $T_0(\mathbf{p})$ is then integrated to yield an expression for the original function:

$$T_0(\mathbf{p}) = \sum_{n=1}^{lN} \phi(\|\mathbf{p} - \mathbf{p}_{k(l,n)}\|)_l \alpha_n \tag{17}$$

The unknown coefficients $_l\alpha_n$, $n = 1, 2, \ldots, {}_lN$ are determined by collocation

$$T_0(\mathbf{p}_{k(l,m)}) = \sum_{n=1}^{lN} \phi(\|\mathbf{p}_{k(l,m)} - \mathbf{p}_{k(l,n)}\|)_l \alpha_n, \quad \mathbf{p}_{k(l,m)} \in {}_l\Omega, \quad m = 1,2,\ldots,{}_lN. \tag{18}$$

The system of equations can be written in a matrix vector notation

$${}_l\mathbf{T} = {}_l\mathbf{\Phi}_l\boldsymbol{\alpha}; \quad {}_l\Phi_{mn} = \phi\left(\|\mathbf{p}_{k(l,m)} - \mathbf{p}_{k(l,n)}\|\right), \quad {}_l\mathbf{T}(m) = T_0(\mathbf{p}_{k(l,m)}), \tag{19}$$

where $_l\boldsymbol{\alpha} = [{}_l\alpha_1 \, {}_l\alpha_2 \cdots {}_lN\alpha_n]^T$ and $_l\Phi_{mn}$ is the entry element of the matrix of $_l\mathbf{\Phi}$ at m row and n column. The coefficient $_l\boldsymbol{\alpha}$ can be represented by inverting system (19)

$${}_l\boldsymbol{\alpha} = {}_l\mathbf{\Phi}^{-1}{}_l\mathbf{T}. \tag{20}$$

By taking into account the expressions for the calculation of the coefficients $_l\boldsymbol{\alpha}$ the indirect collocation representation of function $T_0(\mathbf{p})$ on subdomain $_l\Omega$ can be expressed as

$$T_0(\mathbf{p}) = \sum_{n=1}^{lN} \sum_{m=1}^{lN} \phi(\|\mathbf{p} - \mathbf{p}_{k(l,n)}\|)_l \Phi_{mn}^{-1} T_0(\mathbf{p}_{k(l,m)}) \tag{21}$$

Then the operation of the Laplacian on temperature $T_0(\mathbf{p})$ at initial time at the global point $\mathbf{p}$ on sub-domain $_l\Omega$, $\nabla^2 T_0(\mathbf{p})$, can be expressed as

$$\nabla^2 T_0(\mathbf{p}) = \sum_{n=1}^{lN} \sum_{m=1}^{lN} \psi(\|\mathbf{p} - \mathbf{p}_{k(l,n)}\|)_l \Phi_{mn}^{-1} T_0(\mathbf{p}_{k(l,m)}) \tag{22}$$

As a result, every quantity in (5) is known except the temperature at point $\mathbf{p}_k$ $k = 1,2,\ldots,N$ at $t = t_0 + \Delta t$, and it can be calculated by

$$\hat{T}(\mathbf{p}_k, t_0 + \Delta t) = T_0(\mathbf{p}_k) + \Delta t \sum_{n=1}^{lN} \sum_{m=1}^{lN} \psi(\|\mathbf{p}_k - \mathbf{p}_{k(l,n)}\|)_l \Phi_{mn}^{-1} T_0(\mathbf{p}_{k(l,m)}). \tag{23}$$

This completes the formulation of the LMAPS.

3.3. LDRBFCM

In this approach, the formulation of the problem starts with the representation of initial conditions with RBFs. The derivatives are then calculated by differentiation of the RBF representation. Assume that the temperature is represented on each of the sub-domains by $_lN$ RBF's $\psi(\|\mathbf{p} - \mathbf{p}_{k(l,n)}\|)$ and $_l\alpha, n = 1,2,\ldots,{}_lN$; i.e. ,

$$T_0(\mathbf{p}) = \sum_{n=1}^{lN} \psi(\|\mathbf{p} - \mathbf{p}_{k(l,n)}\|)_l \alpha_n, \quad \mathbf{p} \in {}_l\Omega. \tag{24}$$

It follows that

$$\nabla^2 T_0(\mathbf{p}) = \sum_{n=1}^{lN} \nabla^2 \psi(\|\mathbf{p} - \mathbf{p}_{k(l,n)}\|)_l \alpha_n, \quad \mathbf{p} \in {}_l\Omega. \tag{25}$$

The coefficients $_l\alpha$ are determined by collocation

$$T_0(\mathbf{p}_{k(l,m)}) = \sum_{n=1}^{lN} \psi(\|\mathbf{p}_{k(l,m)} - \mathbf{p}_{k(l,n)}\|)_l \alpha_n, \quad \mathbf{p}_{k(l,m)} \in {}_l\Omega, \quad m = 1,2,\ldots,{}_lN. \tag{26}$$

This can be written as

$${}_l\mathbf{T} = {}_l\mathbf{\Psi}_l\boldsymbol{\alpha}, \tag{27}$$

with the matrix element $_l\Psi_{mn}$ of the matrix $_l\mathbf{\Psi}$ denoted as

$${}_l\Psi_{mn} = \psi(\|\mathbf{p}_{k(l,m)} - \mathbf{p}_{k(l,n)}\|). \tag{28}$$

We determine the coefficients $_l\alpha$ by inverting the matrix $_l\mathbf{\Psi}$ (i.e. $_l\mathbf{\Psi}^{-1}{}_l\mathbf{\Psi} = {}_l\mathbf{I}$)

$${}_l\boldsymbol{\alpha} = {}_l\mathbf{\Psi}^{-1}{}_l\mathbf{T} \tag{29}$$

with the matrix element $(_l\mathbf{\Psi}^{-1})_{mn}$ of the matrix $_l\mathbf{\Psi}^{-1}$ denoted as $_l\Psi_{mn}^{-1}$, which implies that for $\mathbf{p} \in {}_l\Omega$

$$T_0(\mathbf{p}) = \sum_{n=1}^{lN} \sum_{m=1}^{lN} \psi(\|\mathbf{p} - \mathbf{p}_{k(l,n)}\|)_l \Psi_{mn}^{-1} T_0(\mathbf{p}_{k(l,m)}), \tag{30}$$

and

$$\nabla^2 T_0(\mathbf{p}) = \sum_{n=1}^{lN} \sum_{m=1}^{lN} \nabla^2 \psi(\|\mathbf{p} - \mathbf{p}_{k(l,n)}\|)_l \Psi_{mn}^{-1} T_0(\mathbf{p}_{k(l,m)}). \tag{31}$$

Let $\phi(r) = \nabla^2 \psi(r)$. Then the operation of the Laplacian on temperature at initial time at the global point $\mathbf{p}, \nabla^2 T_0(\mathbf{p})$ is

obtained as

$$\nabla^2 T_0(\mathbf{p}) = \sum_{n=1}^{_lN} \sum_{m=1}^{_lN} \varphi(\|\mathbf{p}-\mathbf{p}_{k(l,n)}\|)_l \mathbf{\Psi}_{mn}^{-1} T_0(\mathbf{p}_{k(l,m)}). \tag{32}$$

As a result, every quantity in the right hand side of (5) is known except the temperature at point $\mathbf{p}_k$, $k=1,2,...,N$ at $t=t_0+\Delta t$, and it can be calculated by

$$\hat{T}(\mathbf{p}_k,t_0+\Delta t) = T_0(\mathbf{p}_k)+\Delta t \sum_{n=1}^{_lN} \sum_{m=1}^{_lN} \varphi(\|\mathbf{p}_k-\mathbf{p}_{k(l,n)}\|)_l \mathbf{\Psi}_{mn}^{-1} T_0(\mathbf{p}_{k(l,m)}). \tag{33}$$

This completes the formulation of the LDRBFCM.

3.4. LIRBFCM

In the indirect RBF collocation method, the formulation of the problem starts with the representation of the second derivatives of the original function (initial temperature field) with RBFs, the original function is then obtained by integration. In 2D case, suppose the original function is the initial temperature field $T_0(x,y)$, and its partial derivatives $\partial^2 T_0(x,y)/\partial x^2$ and $\partial^2 T_0(x,y)/\partial y^2$ are to be approximated. To illustrate the procedure, the detail of IRBFCM to obtain $\partial^2 T_0(x,y)/\partial x^2$ is described as follows: assume the second partial derivate of $T_0(x,y)$ with respect to the variable $\xi=x,y$ is first approximated in terms of RBFs, i.e.

$$\frac{\partial^2 T_0(\mathbf{p})}{\partial \xi^2} = \sum_{n=1}^{_lN} \psi(\|\mathbf{p}-\mathbf{p}_{k(l,n)}\|)_l \alpha_n, \quad \mathbf{p} \in {}_l\Omega. \tag{34}$$

Assume

$$\varphi_{k(l,n)}^{\xi\xi}(\mathbf{p}) = \iint \psi(\|\mathbf{p}-\mathbf{p}_{k(l,n)}\|)d\xi d\xi. \tag{35}$$

Note that $\varphi_{k(l,n)}^{\xi\xi}$ in (35) is no longer a radial basis function. The original temperature field can be given by

$$T_0(\mathbf{p}) = \sum_{n=1}^{_lN} \varphi_{k(l,n)}^{\xi\xi}(\mathbf{p})_l \alpha_n, \quad \mathbf{p} \in {}_l\Omega, \tag{36}$$

The coefficients $_l\alpha$ are determined by collocation

$$T_0(\mathbf{p}_{k(l,m)}) = \sum_{n=1}^{_lN} \varphi_{k(l,n)}^{\xi\xi}(\mathbf{p}_{k(l,m)})_l \alpha_n, \quad \mathbf{p}_{k(l,m)} \in {}_l\Omega, \quad m=1,2,...,_lN. \tag{37}$$

This can be written as a $_lN \times _lN$ linear system

$$_l\mathbf{T} = {}_l^{\xi\xi}\mathbf{\Phi}_l\boldsymbol{\alpha}, \tag{38}$$

with the element $_l^{\xi\xi}\mathbf{\Phi}_{mn}$ of the matrix $_l^{\xi\xi}\mathbf{\Phi}$ defined as

$$_l^{\xi\xi}\mathbf{\Phi}_{mn} = \varphi_{k(l,n)}^{\xi\xi}(\mathbf{p}_{k(l,m)}), \quad _l\mathbf{T}(m) = T_0(\mathbf{p}_{k(l,m)}), \quad m=1,\cdots,_lN, \tag{39}$$

where $m=1,...,_lN$. By taking into account the expressions for the calculation of the coefficients $_l\boldsymbol{\alpha}$ the indirect collocation representation of function $T_0(\mathbf{p})$ on subdomain $_l\Omega$ can be expressed as

$$T_0(\mathbf{p}) = \sum_{n=1}^{_lN} \sum_{m=1}^{_lN} \varphi_{k(l,n)}^{\xi\xi}(\mathbf{p})_l^{\xi\xi}\mathbf{\Phi}_{mn}^{-1} T_0(\mathbf{p}_{k(l,m)}) \tag{40}$$

The spatial second derivative of $T_0(\mathbf{p})$ on subdomain $_l\Omega$ can be expressed as

$$\frac{\partial^2 T_0(\mathbf{p})}{\partial \xi^2} = \sum_{n=1}^{_lN} \sum_{m=1}^{_lN} \psi(\|\mathbf{p}-\mathbf{p}_{k(l,n)}\|)_l^{\xi\xi}\mathbf{\Phi}_{mn}^{-1} T_0(\mathbf{p}_{k(l,m)}). \tag{41}$$

Thus, the second partial derivative of $T_0(x,y)$ with respect to the variable x and y can be approximated as

$$\frac{\partial^2 T_0(\mathbf{p})}{\partial x^2} = \sum_{n=1}^{_lN} \sum_{m=1}^{_lN} \psi(\|\mathbf{p}-\mathbf{p}_{k(l,n)}\|)_l^{xx}\mathbf{\Phi}_{mn}^{-1} T_0(\mathbf{p}_{k(l,m)}),$$

$$\frac{\partial^2 T_0(\mathbf{p})}{\partial y^2} = \sum_{n=1}^{_lN} \sum_{m=1}^{_lN} \psi(\|\mathbf{p}-\mathbf{p}_{k(l,n)}\|)_l^{yy}\mathbf{\Phi}_{mn}^{-1} T_0(\mathbf{p}_{k(l,m)}). \tag{42}$$

The operation of the Laplacian on temperature at initial time at the global point $\mathbf{p}, \nabla^2 T_0(\mathbf{p})$, is obtained as

$$\nabla^2 T_0(\mathbf{p}) = \frac{\partial^2 T_0(\mathbf{p})}{\partial x^2} + \frac{\partial^2 T_0(\mathbf{p})}{\partial y^2}$$

$$= \sum_{n=1}^{_lN} \sum_{m=1}^{_lN} \psi(\|\mathbf{p}-\mathbf{p}_{k(l,n)}\|)(_l^{xx}\mathbf{\Phi}_{mn}^{-1} + {}_l^{yy}\mathbf{\Phi}_{mn}^{-1})T_0(\mathbf{p}_{k(l,m)}), \tag{43}$$

As a result, every quantity in the right hand side of (5) is known except the temperature at point $\mathbf{p}_k$, $k=1,2,...,N$ at $t=t_0+\Delta t$, and it can be approximated as

$$\hat{T}(\mathbf{p}_k,t_0+\Delta t) = T_0(\mathbf{p}_k)+\Delta t \sum_{n=1}^{_lN} \sum_{m=1}^{_lN} \psi(\|\mathbf{p}_k-\mathbf{p}_{k(l,n)}\|)(_l^{xx}\mathbf{\Phi}_{nm}^{-1}$$

$$+ {}_l^{yy}\mathbf{\Phi}_{nm}^{-1})T_0(\mathbf{p}_{k(l,m)}). \tag{44}$$

This completes the formulation of the LIRBFCM.

4. Numerical results

Through this section, we investigate the performance of the three explicit local meshless methods that can be implemented on evenly or randomly distributed nodes. The computer program has been coded in double precision using GNU Fortran compiler. All numerical results have been run on an Intel Core 2 2.66 GHz 64 bits computer.

The similar multiquadrics scaling technique as in [39] is introduced to alleviate the difficulty of choosing shape parameter in multiquadrics. The scaling parameter r_0 is the maximum nodal distance in the sub-domain

$$r_0 = \max_{1 \le i,j \le {}_lN} r_{ij} = \sqrt{(x_i-x_j)^2 + (y_i-y_j)^2}, \quad \mathbf{p}_i = (x_i,y_i), \quad \mathbf{p}_j = (x_j,y_j) \in {}_l\Omega. \tag{45}$$

The parameter c in all RBFs and corresponding derivatives and integrations are replaced by cr_0. Hence, a large shape parameter of multiquadrics RBF can be used in the numerical implementation, in this paper $c=100$ is used.

For both uniform and non-uniform node arrangement, we leave out the corner points for simplicity. The profile of 51×51 uniformly distributed nodes is shown on the left of Fig. 2. The random nodes are generated from the uniform nodes through the following transformation:

$$\xi_i = \xi_i + c_{rand}\varepsilon r_{min}, \tag{46}$$
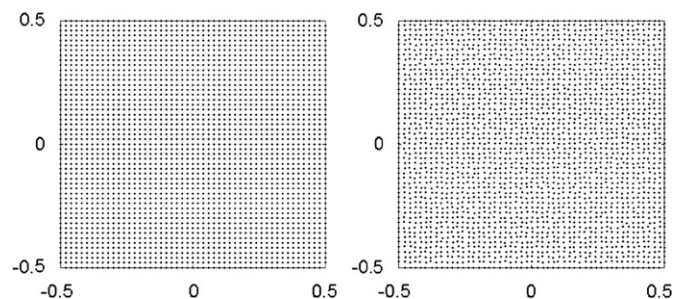
Fig. 2. The 51×51 uniformly distributed nodes on the left, and the randomly distributed nodes with random displacement factor $\varepsilon = 0.2$ on the right.

where ξ_i is coordinate of node $\mathbf{p}_i = (x_i, y_i)$, c_{rand} is a random number between 0 to 1, r_{min} denotes the minimum distance among different uniform points, ε stands for a displacement factor. The profile of 51×51 randomly distributed nodes with displacement factor $\varepsilon = 0.2$ is shown on the right of Fig. 2. Larger displacement factor generates increasingly random node arrangement. The parameter $_lN$ stands for the number of points in the local sub-domain: $_lN = 5$ is used throughout this paper, Δh stands for the minimum distance among the given nodes.

Example. Let domain Ω be unit square $[-0.5, 0.5]^2$. Consider diffusion equation

$$\frac{\partial T}{\partial t}(x,y,t) = \nabla^2 T(x,y,t), \quad (x,y) \in \Omega, \, t > 0, \tag{47}$$

with initial condition

$$T(x,y,0) = 1, \quad (x,y) \in \Omega \cup \Gamma \tag{48}$$

and Dirichelt jump boundary condition

$$T(x,y,t) = 0, \quad (x,y) \in \Gamma, t > 0. \tag{49}$$

The analytical temperature is given by [41]

$$T(x,y,t) = \frac{16}{\pi^2} T_{ana}(x,t) T_{ana}(y,t) \tag{50}$$

with $\xi = x, y$,

$$T_{ana}(\xi,t) = \sum_{i=0}^{\infty} \frac{(-1)^i \exp[-(2i+1)^2 \pi^2 t] \cos[(2i+1)\pi\xi]}{2i+1}. \tag{51}$$

The absolute error, the maximum absolute error and the average error of the numerical solution at time t are defined as

$$T_{abs} = |\hat{T}(\mathbf{p}_k,t) - T(\mathbf{p}_k,t)|, \quad k = 1,2,\ldots,N,$$

$$T_{max} = \max_{1 \le k \le N} |\hat{T}(\mathbf{p}_k,t) - T(\mathbf{p}_k,t)|,$$
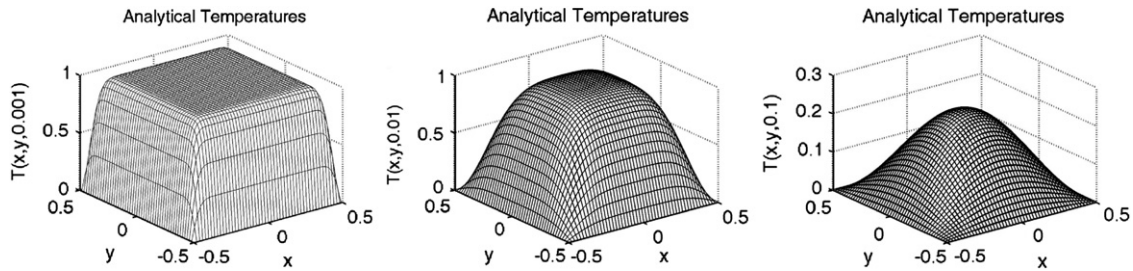
Fig. 3. The analytical temperatures at time $t = 10^{-3}$, $t = 10^{-2}$ and $t = 10^{-1}$ from left to right.
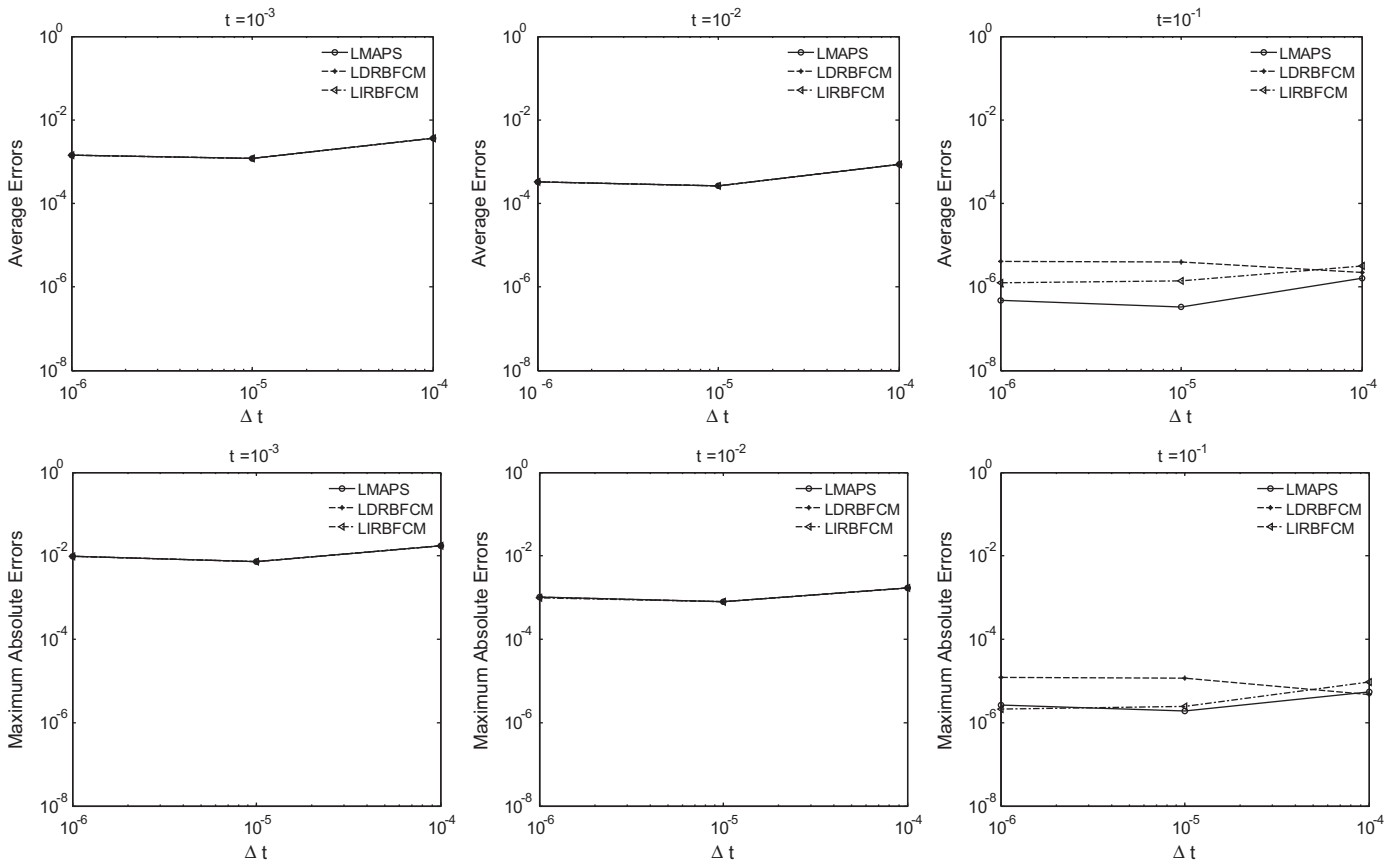
Fig. 4. Errors as a function of size of time step at different time with 51×51 uniform nodes.

$$T_{avg} = \frac{1}{N} \sum_{k=1}^{N} |\hat{T}(\mathbf{p}_k, t) - T(\mathbf{p}_k, t)|, \qquad (52)$$

where $\hat{T}$ and T stand for numerical and analytical solutions, respectively. Fig. 3 shows the profiles of the analytical solutions at $t=0.001$, 0.01 and $t=0.1$. At $t=0.001$, the temperature field experiences big jump near boundary area, and this is very challenging and interesting state to approximate. When $t=0.01$, the temperature fields become smother. The accuracy of approximations at this time appears higher.

Fig. 4 shows the accuracy of the solution as a function of the time step length. The average errors and maximum absolute errors are calculated on 51×51 evenly distributed nodes at $t=0.001$, 0.01 and

0.1. For the short times $t=0.001$ and $t=0.01$, all three methods represent the same accuracy on both average and maximum errors, and the errors can be significantly improved when changing the time step length from 10^{-4} to 10^{-5}. For longer times such as $t=0.1$, all errors are extremely small, and there is no much difference among these three methods. On the other hand, when we decrease the size of the time steps to 10^{-6}, the errors of all three methods are not decreasing anymore. This is because for further decrease of the error, also space discretization needs to be refined.

Fig. 5 shows the stability of these methods with respect to the minimum distance among the given nodes, where in this figure the size of time steps is chosen as $\Delta t = 10^{-5}$, and time $t=0.001$, 0.01 and 0.1. One can observe the improvement of the accuracy with denser
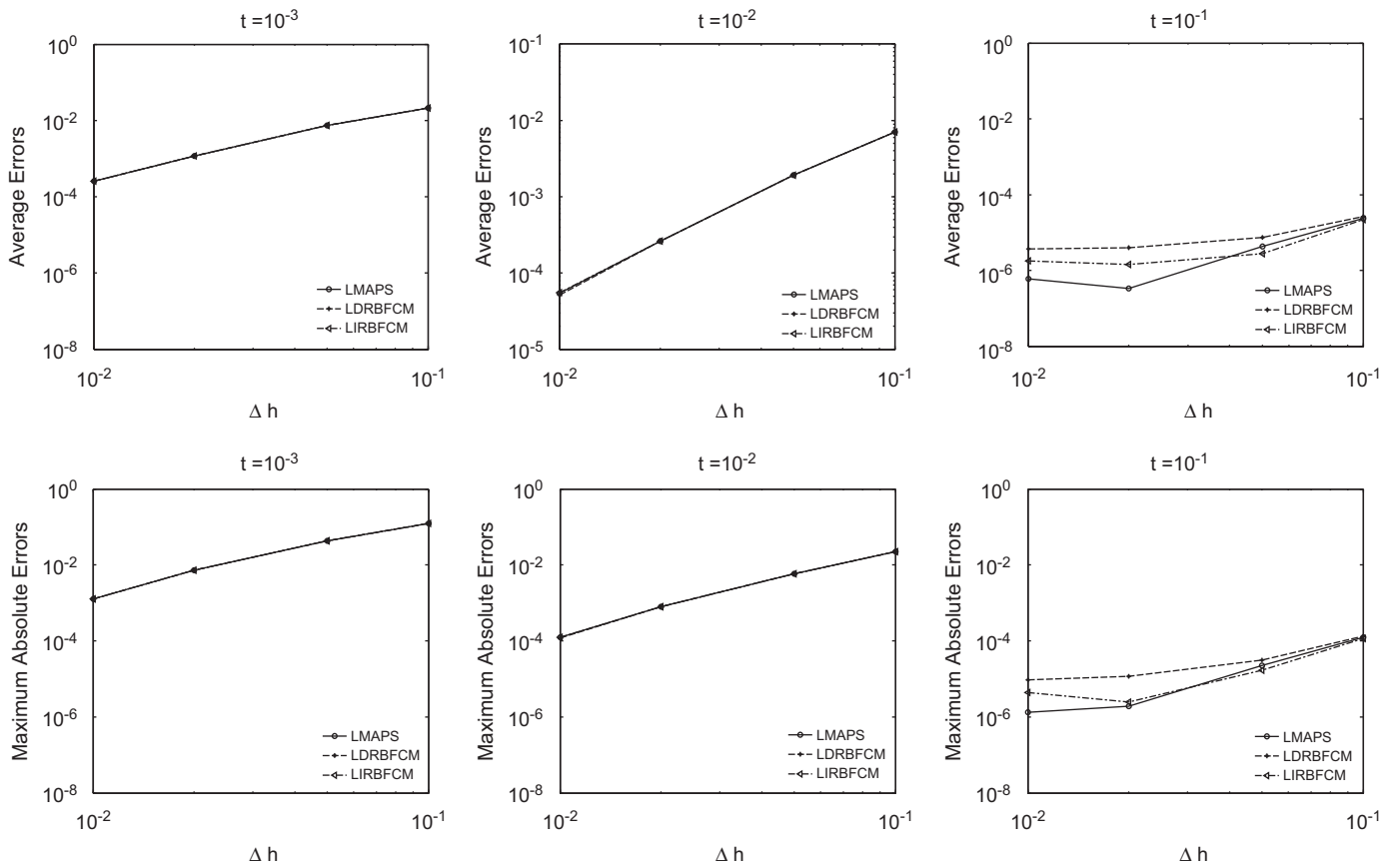
Fig. 5. Errors as a function of minimum distance between nodes at different time with the time step $\Delta t = 10^{-5}$.
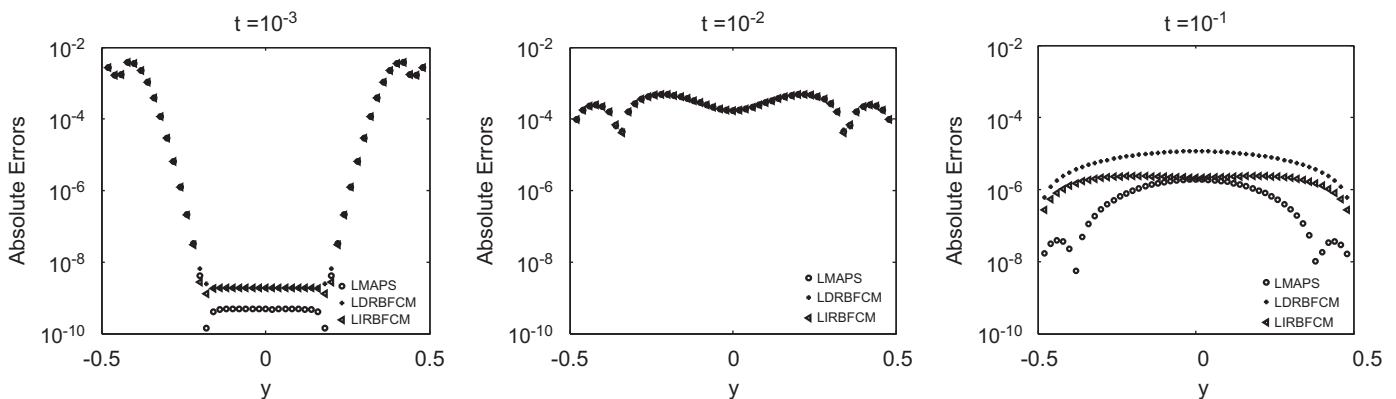
Fig. 6. The absolute errors in y direction for $x=0.0$, with 51×51 uniform nodes and the time step length $\Delta t = 10^{-5}$, at different time.

nodes using all three methods. Therefore, all methods give very close accuracy except when the time is larger. As we see from Fig. 4, for $t=0.1$, the LDRBFCM gives slightly larger errors than the LMAPS and the LIRBFCM, but there is no meaningful difference among the results since all the errors are very small.

Fig. 6 shows the absolute errors of the temperature at time $t=0.0001$, 0.001, 0.01 and $t=0.1$ at cross section $(0, y)$, where $y=[-0.5, 0.5]$. At the time $t=0.001$ a very challenging temperature state occurs where the temperature experiences jump near boundary and is difficult to approximate. As we expect, the absolute errors near boundary nodes are much larger than at the center nodes. All errors using the three methods are very small at this time. The errors at central area are increasing as a function of time, and the errors at near boundary area are decreasing. For $t=0.01$ and 0.1, the errors near boundary nodes

are smaller, there are two reasons: the analytical temperature field becomes smoother, and the temperature at the center point is higher than at the boundaries. Overall, the accuracy of all three methods is approximately the same.

In Fig. 7 we show the profiles of the average errors and maximum absolute errors as a function of time using three methods with 51×51 evenly distributed nodes, where $\Delta t=10^{-5}$. We compare the errors based on the given interior nodes at time t from 0 to 0.1. The errors are decreasing as t becomes larger. One can observe numerically the LMAPS and the LIRBFCM methods give slightly better accuracy than the LDRBFCM when t is larger, but practically there is no difference. When the time is small, all three methods perform practically the same.

Fig. 8 shows the profiles of the average errors and the maximum errors which were obtained on 51×51 non-uniform
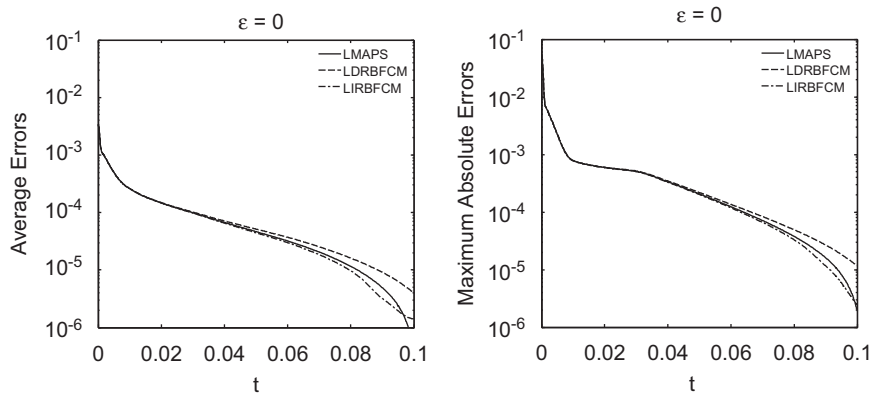
Fig. 7. The average and the maximum errors as a function of time with 51×51 uniform nodes using the time step $\Delta t=10^{-5}$.
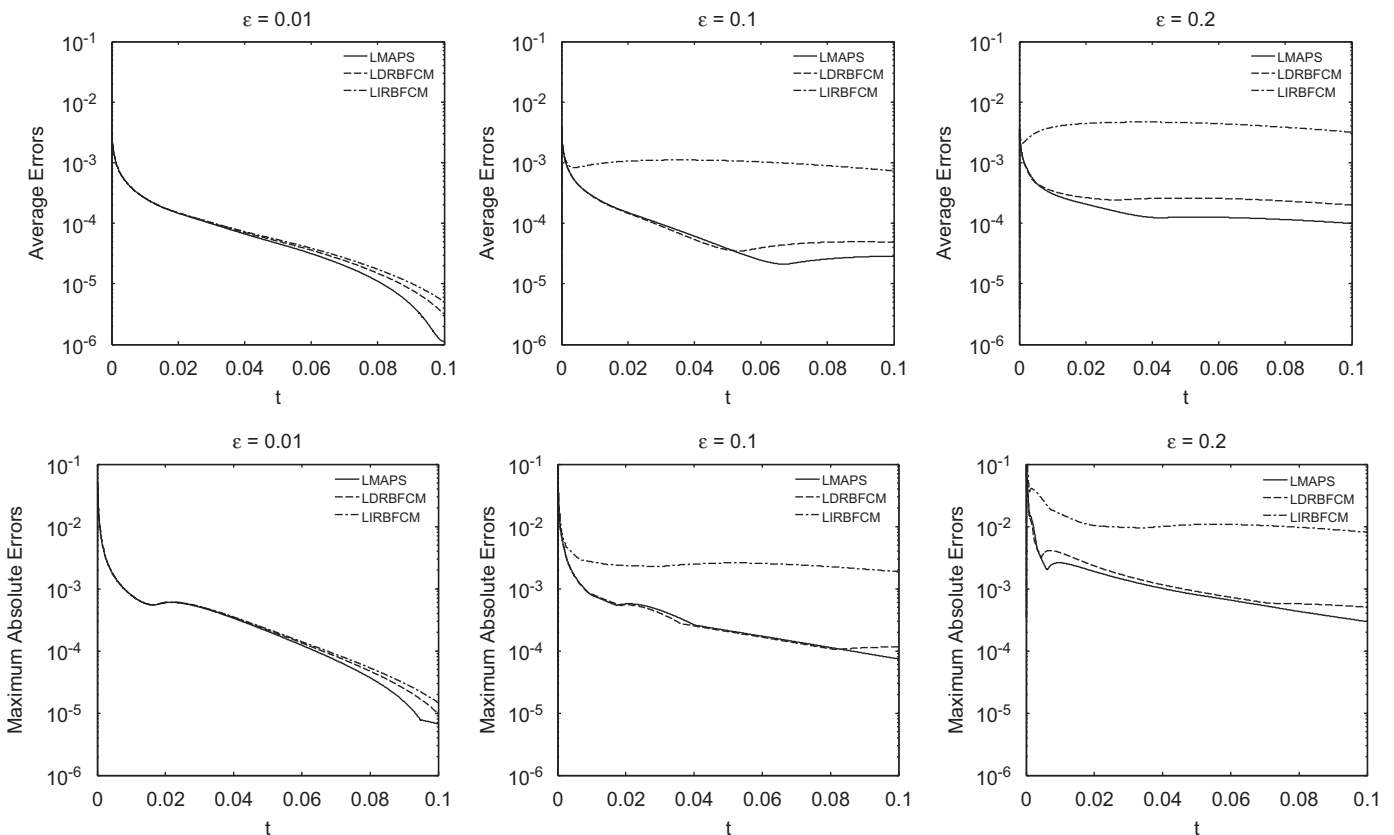
Fig. 8. Errors as a function of time with 51×51 random nodes associated with a different random displacement factor $\varepsilon=0.01, 0.1, 0.2$ with time step $\Delta t=10^{-5}$.

nodes with different displacement factors $\varepsilon = 0.01$, 0.1, 0.2. A larger ε generates increasingly random nodes which gives different numerical behaviors. For $\varepsilon = 0.01$, the errors of the LIRBFCM and the LDRBFCM are slightly increased compared with the evenly distributed node arrangement, but for larger ε, the LIRBFCM diverges very quickly.

Figs. 9 and 10 represent the absolute errors using these three explicit methods for time $t = 0.001$, 0.01 and 0.1 where the errors are calculated on 51×51 evenly distributed nodes and on 51×51 non-uniformly distributed nodes with $\varepsilon = 0.2$. The results are obtained based on both kinds of nodes. For the smaller time, all errors show the same accuracy and the errors at the corner points are relatively large since the neighbor of the corner points includes only two boundary nodes in the evenly distributed node arrangement. For non-evenly distributed nodes, the LDRBFCM and the LMAPS perform much better than the LIRBFCM.

All the methods are made locally over a set of overlapping sub-domains and the time stepping is performed in an explicit way, the radial basis function collocation techniques are used in sub-domains, small systems of linear equations have to be solved in each time step for each node and associated sub-domain. The LIRBFCM takes much longer CPU time compared with other two methods since the partial derivatives of original temperature fields on each direction are needed, which requires two inverse matrices at each time step. The matrix on the left-hand side of five-noded small system is symmetric, non-negative. Due to the difficulty of obtaining closed-form particular solutions for complicated operator and multi-dimensional space, the LMAPS may not be available for MQ. However, in this case, other radial basis functions such as polyharmonic splines can be selected as the basis function. The integrations of RBFs on each direction in the domain are needed for the LIRBFCM, which also yields higher order integrations that may not be available for some RBFs, but the LDRBFCM can always be used by direct differentiations of the RBFs. Thus, the LDRBFCM can be considered as a preferable choice in general case.

5. Conclusions

The present paper represents one of the rare publications where different meshless methods are compared at the same test. Three kinds of localized meshless methods were compared for
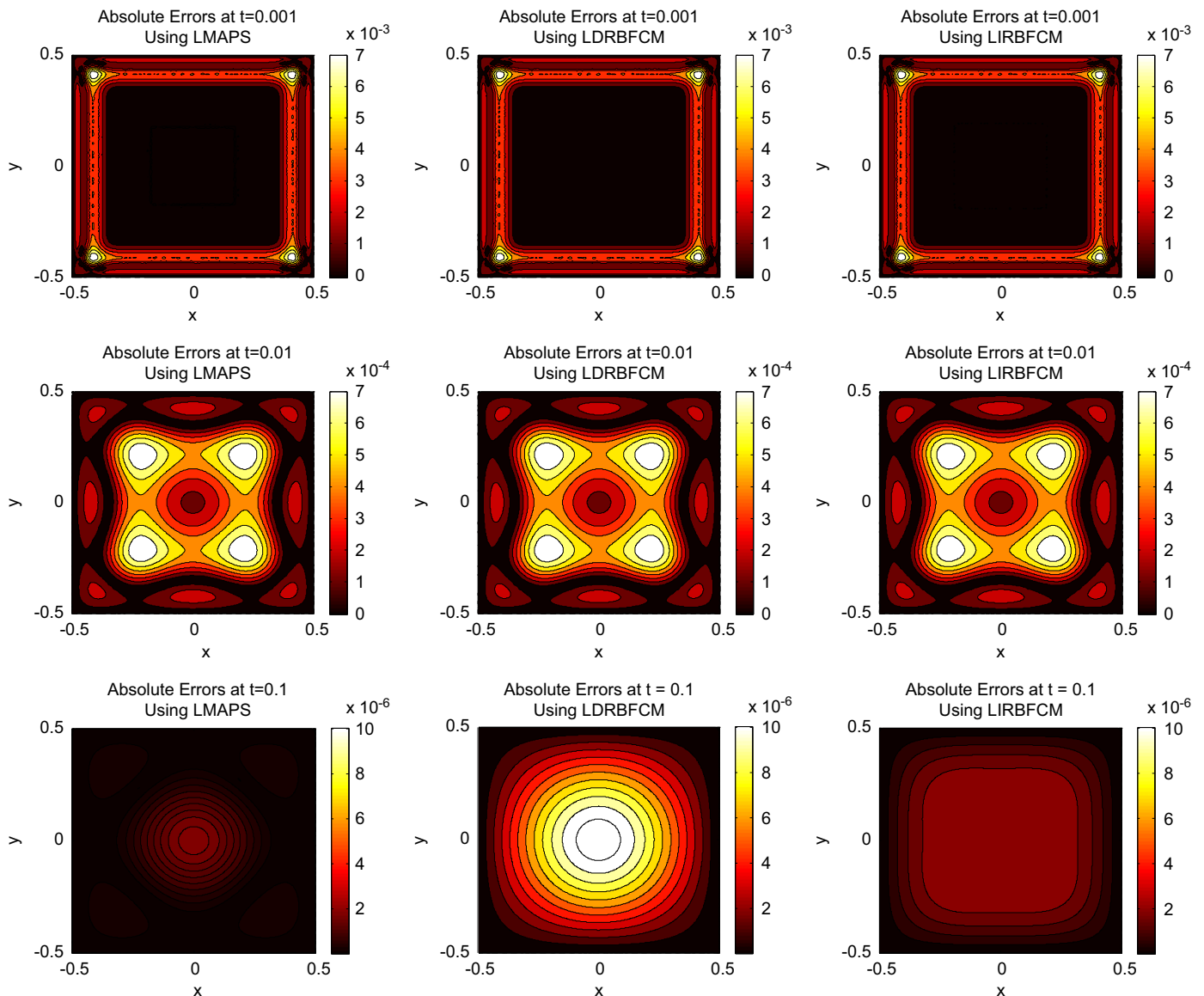
Fig. 9. The approximate temperature field at $t = 10^{-3}$, 10^{-2}, 10^{-1} where 51×51 uniform nodes and time step $\Delta t = 10^{-5}$.
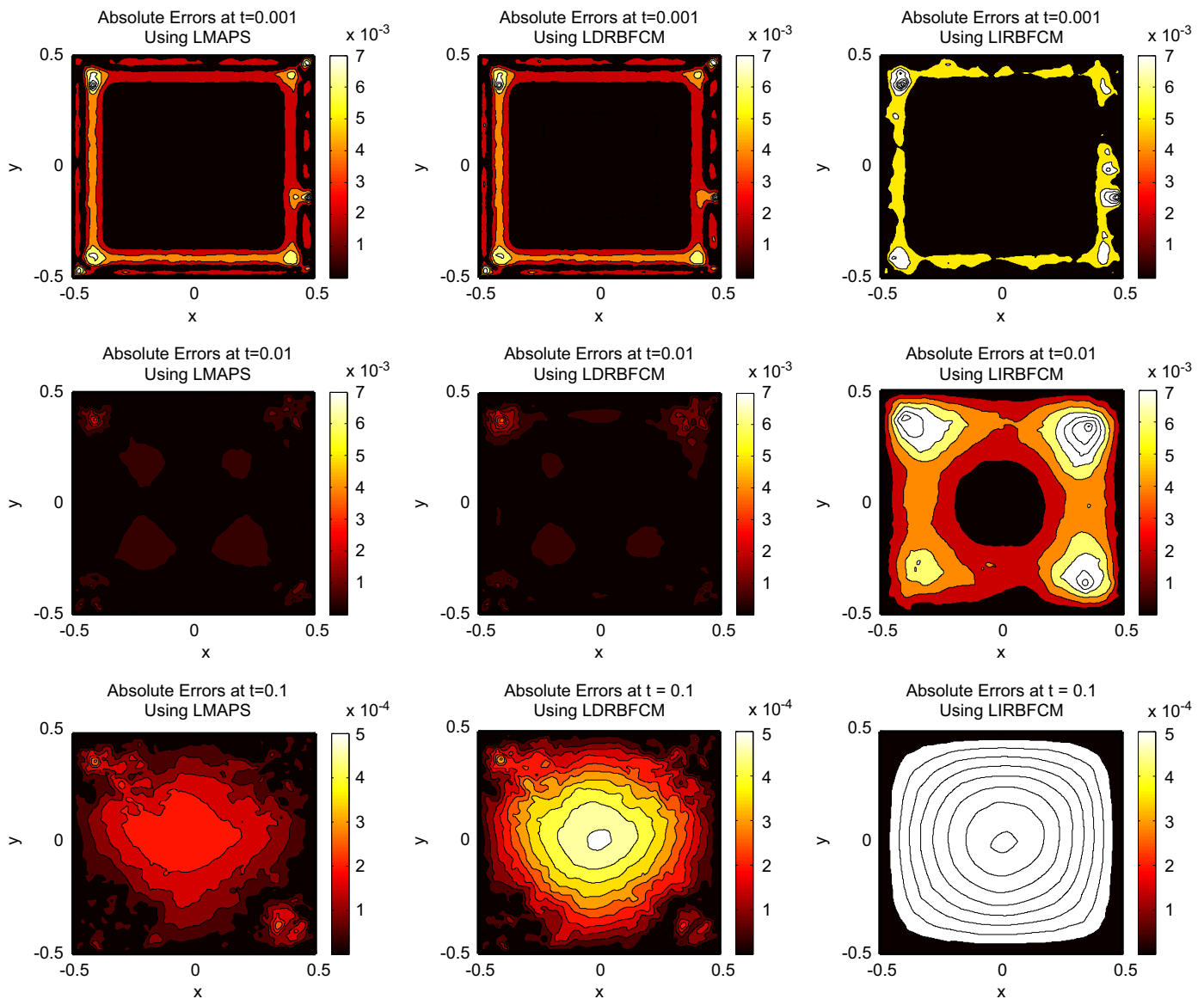
Fig. 10. The approximate temperature fields at $t = 10^{-3}$, 10^{-2}, 10^{-1} with 51×51 random nodes with $\varepsilon = 0.2$ and time step $\Delta t = 10^{-5}$.

Dirichlet jump problem for diffusion equation based on both evenly and non-evenly node distributions: the LMAPS, the LDRBFCM and the LIRBFCM. The LDRBFCM interpolates analytical function using RBFs, the LIRBFCM interpolates the second derivatives of analytical function using RBFs, and the LMAPS interpolate the Laplacian of analytical function using RBFs. The numerical performances of all methods show high accuracy and the improvement of the accuracies with denser nodes and the smaller time step length. On the other hand, the LMAPS and the LIRBFCM give slightly better results for larger time and even node distribution. For non-even node arrangement problems, the LMAPS and the LDRBFCM are more stable.

References

[1] Atluri SN, Shen S. The meshless method. Forsyth: Tech Science Press; 2002.
[2] Fasshauer GE. Meshfree application method with Matlab. Interdiscilinary Mathematical Sciences 2007;6.
[3] Liu GR. Mesh free methods: moving beyond the finite element method. Boca Raton: CRC Press; 2003.
[4] Mai-Duy N, Tran-Cong T. Numerical solution of Navier–Stokes equations using multiquadric radial basis function networks. Neural Networks 2001;14:185–99.
[5] Atluri SN, Shen S. The meshless local Petrov–Galerkin (MLPG) method. Encino: Tech Science Press; 2002.
[6] Atluri SN. The meshless method (MLPG) for domain and BIE discretization. Forsyth: Tech Science Press; 2004.
[7] Liu GR, Dai KY, Lim KM, Gu YT. A point interpolation mesh free method for static and frequency analysis of two-dimensional piezoelectric structures. Comp Mech 2002;29:510–9.
[8] Buhmann MD. Radial basis functions: theory and implementations. Cambridge University Press; 2003.
[9] Chen W, New RBF. Collocation schemes and kernel RBFs with applications. Lect Notes Comput Sci Eng 2002;26:75–86.

[10] Šarler B. From global to local radial basis function collocation method for transport phenomena. In: Leitao V MA, Alves CJS, Armando-Duarte C, editors. Advances in Meshfree Techniques, Computer Methods in Applied Science; 2007. p. 257–82.

[11] Franke J. Scattered data interpolation: tests of some methods. Math Comput. 1982;48:181–200.

[12] Kansa EJ. Multiquadrics—a scattered data approximation scheme with application to computational fluid dynamics, part I. Surface approximations and partial derivative estimates. Comput Math Appl 1990;19:127–45.

[13] Kansa EJ. Multiquadrics—a scattered data approximation scheme with applications to computational fluid dynamics, part II. Solutions to parabolic, hyperbolic and elliptic partial differential equations. Comput Math Appl 1990;19:147–61.

[14] Zerroukat M, Power H, Chen CS. A numerical method for heat transfer problems using collocation and radial basis functions. Int J Numer Methods Eng 1998;42:1263–78.

[15] Šarler B, Gobin D, Goyeau B, Perko J, Power H. Natural convection in porous media-dual reciprocity boundary element method solution of the Darcy model. Int J Numer Methods Fluids. 2000;33:279–312.

[16] Chantasiriwan S. Performance of Multiquadric collocation method in solving lid-driven cavity flow problem with low Reynolds number. Comput Model Eng Sci 2006;15:137–46.

[17] Šarler B. A radial basis function collocation approach in computational fluid dynamics. Comput Model Eng Sci 2005;7:185–93.

[18] Hardy RL. Least square prediction. Photogrammetric Eng Remote Sens. 1977;43:475–92.

[19] Kansa EJ, Hon YC. Circumventing the ill-conditioning problem with multiquadric radial basis functions: applications to elliptic partial differential equations. Comput Math Appl 2000;39:123–37.

[20] Hon YC, Schaback R, Zhou X. An adaptive greedy algorithm for solving large RBF collocation problems. Numer Algor 2003;32:13–25.

[21] Ling L, Schaback R. Stable and convergent unsymmetric meshless collocation methods. SIAM J Numer Anal 2008;46:1097–115.

[22] Huang CS, Lee CF, Cheng A. Error estimate, optimal shape factor, and high precision computation of multiquadric collocation method. Eng Anal Bound Elem 2007;31:614–23.

[23] Libre NA, Emdadi A, Kansa EJ, Rahimian M, Shekarchi M. A stabilized RBF collocation scheme for Neumann type boundary value problems. Comput Model Eng Sci 2008;24:61–80.

[24] Mai-Duy N, Tran-Cong T. Mesh-free radial basis function network methods with domain decomposition for approximation of functions and numerical solution of Poisson's equation. Eng Anal Bound Elem 2002;26:133–56.

[25] Chen CS, Ganesh M, Golberg MA, Cheng AHD. Multilevel compact radial basis functions based computational scheme for some elliptic problems. Comput Math Appl 2002;43:359–78.

[26] Shu C, Ding H, Yeo KS. Local radial basis function-based differential quadrature method and its application to solve two dimensional incompressible Navier–Stokes equations. Comput Methods Appl Mech Eng 2003;192:941–54.

[27] Lee CK, Liu X, Fan SC. Local multiquadric approximation for solving boundary value problems. Comput Mech 2003;30:396–409.

[28] Šarler B, Vertnik R. Meshfree explicit local radial basis function collocation method for diffusion problems. Comput Math Appl 2006:1269–82.

[29] Chen CS, Yao GM. A localized approach for the method of approximate particular solutions, Book of abstracts. In: Atluri SN, Šarler B, editors. Proceedings of the fifth ICCES international symposium on meshless and other novel computational methods. Ljubljana, Slovenia: University of Nova Gorica; 2009. p. 2.

[30] Chen CS, Fan CM, Wen PH . The method of approximate particular solutions for solving certain partial differential equations, Numerical Methods for Partial Differential Equations, in press, doi:10.1002/num.20631.

[31] Vertnik R, Šarler B. Meshless local radial basis function collocation method for convective-diffusive solid–liquid phase change problems. Int J Numer Methods Heat Fluid Flow 2006;16:617–40.

[32] Vertnik R, Založnik M, Šarler B. Solution of transient direct-chill aluminum billet casting problem with simulations material and interphase moving boundaries by a meshless method. Eng Anal Bound Elem 2006;30:847–55.

[33] Kovačević I, Šarler B. Solution of a phase-field model for dissolution of primary particles in binary aluminum alloys by an r-adaptive mesh-free method. Mater Sci Eng A 2005;413–414:423–8.

[34] Divo E, Kassab AJ. An efficient localized RBF meshless method for fluid flow and conjugate hear transfer. ASME J Heat Transfer 2007;129: 124–36.

[35] Kosec G, Šarler B, Local RBF. Collocation method for Darcy flow. Comput Model Eng Sci 2008;25(3):197–207.

[36] Vertnik R, Šarler B. Solution of incompressible turbulent flow by a mesh-free method. Comput Model Eng Sci 2009;44(1):65–96.

[37] Mai-Duy N, Tran-Cong T. Approximation of function and its derivatives using radial basis function networks. Appl Math Model 2003;27:197–220.

[38] Mai-Duy N, Tran-Cong T. Indirect RBFN method with thin plate splines for numerical solution of differential equations. Comput Model Eng Sci 2003;4:85–102.

[39] Vertnik R. Local collocation method for phase-change problems. Master's thesis, University of Nova Gorica, 2007.

[40] Karageorghis A, Chen CS, Smyrlis Y-S. Matrix decomposition RBF algorithm for solving 3D elliptic problems. Eng Anal Bound Elem 2009;33: 1368–73.

[41] Carlsaw HS, Jaeger JC. Condition of heat in solids. Oxford: Clarendon Press; 1995.